EXPLORING CLAY AND SILICATE-BASED MINERAL PROFILES ALONG PICHAVARAM COASTAL REGION, TAMIL NADU, WITH AVIRIS-NG HYPERSPECTRAL DATA

S. SUDHARSAN[1], R. HEMALATHA[2], S. RADHA[3]

[1]Assistant Professor, [2]Associate Professor, [3]Professor and Vice Principal
[1,2,3]Dept. of ECE,1Rajalakshmi Engineering College, 2,3Sri Sivasubramaniya Nadar College of
Engineering, Chennai, Tamil Nadu, India
[1]sudharsan.s@rajalakshmi.edu.in ,2hemalathar@ssn.edu.in,3radhas@ssn.edu.in

(Received October 21, 2024; revised version accepted November 8, 2024)

ABSTRACT

Hyperspectral Remote Sensing (HRS) is crucial for detecting and mapping the exact position of minerals by analyzing their spectral characteristics in various formations of rock within the Visible Near Infra-Red (VNIR) and Short-Wave Infra-Red (SWIR) range of the electromagnetic radiation spectrum using spaceborne and airborne data. Airborne data availability facilitates the straightforward identification of economically prosperous mineral rich areas. The research has been conducted using the hyperspectral dataset from the Airborne Visible Infrared Imaging Spectrometer Next Generation (AVIRIS-NG) in the Pichavaram area of Chidambaram town, located in the Cuddalore district of Tamil Nadu, India. This study aims to detect minerals by analyzing the spectral reflectance curve of images in conjunction with the USGS Laboratory spectra of minerals included in the ENVI library. This research seeks to identify abundant mineral deposits like vermiculite, antigorite, diopside, rectorite, and ammonio jarosite along the coastal areas. The Spectral Angle Mapper (SAM) and Spectral Feature Fitting (SFF) algorithms are utilized for mapping and analysis—the investigation aimed to identify economically valuable areas with mineral wealth using AVIRIS-NG data. In future work, machine learning models (MLMs) using supervised classifiers can improve the availability and accurate identification of minerals.

KEY WORDS: AVIRIS-NG, SAM, SFF, Hyperspectral Remote Sensing, Clay and Silicate Minerals

0963-0651/23/$5.00

INTRODUCTION AND LITERATURE SURVEY

The use of remote sensing methods has significantly enhanced the field of geology and mineral identification since their inception. Remote sensing images can help geologists differentiate between mineral deposits (Agrawal et al., 2024). Mineral mapping using the old method is time-consuming, intricate, and demanding (Tripathi and Govil, 2019). Precise mineral mapping is essential for identifying valuable mineral deposits and managing geological dangers. Various forms of remote sensing, including airborne and satellite-based methods, provide in-depth data on surface characteristics over vast and hard-to-reach regions (Mishra et al., 2024).

Hyperspectral Imaging (HSI) is the combination of remote sensing and spectroscopy. Since the beginning of evolution, it has become vital to identify, differentiate, and map the earth's surface characteristics according to its chemical composition and structures (Guha, 2020). Each mineral exhibits unique spectral absorption properties at a distinct wavelength determined by its chemical structure and physical attributes (Girija and Sundararajan, 2019). The broader spectral resolution of multispectral remote sensing limits its ability to identify mineral resources. This restriction results in ambiguities in the identification of mineral deposits (Mondal et al., 2022).

Over the past thirty years, advancements in HRS have led to the creation of various spaceborne and airborne sensors like "Advanced Visible Infrared Imaging Spectrometer (AVIRIS), Hyperspectral Digital Imagery Collection Experiment (HYDICE), Hyperspectral Mapper (HM), and Hyperion" (Tripathi and Govil, 2019). Hyperspectral sensors enable the identification and mapping of minerals based on spectral features (Agrawal et al., 2024). According to Peyghambari and Zhang (2021), HRS data has primarily been utilized for geological applications, such as lithology and mineral exploration, ore deposits, surface maps of different materials (rocks and minerals), and image classification of industrial mining.

Low signal-to-noise ratio (SNR), striping, and geometric distortions, including smile and keystone errors, were among the shortcomings of Hyperion and AVIRIS sensors (Tripathi and Govil, 2019). The Jet Propulsion Laboratory, a division of the National Aeronautics and Space Administration (JPL NASA) with ISRO, is developing a potential solution to solve these problems by creating a new advanced airborne sensor called AVIRIS-NG (NASA AVIRIS-NG, 2015 and SAC, 2016). The mission flights were conducted on March 4th, 2018, to acquire satellite images for mineral identification along the coastal regions of Tamil Nadu, India.

Within the 400 nm to 2500 nm range, the AVIRIS-NG sensor offers 425 wavelength channels with exceptional geographical and wavelength clarity. It is specifically made to improve identification, differentiation, and charting capacities. Agrawal et al., (2024), In light of its high SNR, the sensor boasts superior wavelength and geographical clarity than spaceborne sensors, permitting it to acquire an extensive amount of spectrally pristine target pixels

(Mishra et al., 2024). AVIRIS-NG has evolved into the most sophisticated data source for mineral detection and charting in airborne hyperspectral remote sensing (HRS) (Govil et al., 2018; Govil et al.,2019). Some of the research works done by the spaceborne and airborne sensors are discussed.

Oskouei and Babakan (2016) analyzed hyperion data to identify potential minerals like kaolinite and opal in the Lahroud area. The linear mixture model (LMM) is used for data processing; however, identification is challenging because of the Hyperion sensor's poor SNR. Mineral exploration is desirable, considering its cost-effectiveness and time efficiency.

Tripathi and Govil (2019) utilized the AVIRIS-NG data to identify clay minerals in the Jahajpur area. The SAM and SFF algorithms accurately identified valuable mineral locations.

Agrawal et al., (2024) exploited AVIRIS-NG data for mineral detection, employing several MLMs such as "Support Vector Machines (SVM), K Nearest Neighbour (KNN), Decision Tree (DT), Random Forest (RF), Logistic Regression (LR), Artificial Neural Network (ANN), Linear Discriminant Analysis (LDA), and Naïve Bayes (NB)". SAM Classification is applied to establish the reference mineral distribution for various minerals. Conclusions showed that AVIRIS-NG maps prospective mapping zones using Machine learning algorithms (MLA). Kumar et al., (2020) focussed on using spectral enhancement methods and MLA with AVIRIS-NG for automated lithological analysis. Several MLMs were compared, showing that specific models provided higher accuracy and kappa coefficient for identifying minerals such as metabasalt, amphibolite, granite, acidic intrusive, and migmatite.

Priya and Ghosh (2024) identified an abundance of soil clay minerals like "kaolinite, montmorillonite, and illite" using the AVIRIS-NG data. The SFF algorithm was used for the analysis, and results were found to be better and with excellent accuracy in the Udaipur region of Rajasthan. Mondal et al., (2022) combine AVIRIS-NG and Landsat-8 OLI data for mapping minerals in the lithological units of Sittampundi. The Constrained Energy Minimization (CEM) and SAM approaches were utilized for the study. The results indicate that AVIRIS-NG data outperforms Landsat-8 OLI data in mapping metagabbro/mafic minerals.

Mishra et al., (2024) compared aerial AVIRIS-NG and spaceborne PRISMA datasets to map hydrothermally changed minerals in the Jahazpur district of Rajasthan. SAM is used in the research area to detect "talc, soapstone, and kaolinite" minerals. The results indicated that AVIRIS-NG data is more efficient in mapping tiny mineral particles due to its superior spatial resolution and SNR values compared to PRISMA hyperspectral data.

From the above literature, it is evident that AVIRIS-NG data has been used for mineral exploration in different regions using SAM and SFF methods. Due

to its higher SNR with better spatial and spectral resolution, identification becomes easier compared to spaceborne sensors like Hyperion.

The current work aims to use the AVIRIS-NG dataset for mineral mapping in Pichavaram Village near Chidambaram town, located in Cuddalore district in Tamil Nadu, India. This study aims to explore the mineral deposits along the coastal regions using the SAM and SFF methods.

Geological Settings of the Study Area

Tamil Nadu is a significant contributor to the country's mineral resources, and according to a study, it accounts for approximately 50% (79% vermiculite, 65% dunite, 52% molybdenum, 48% garnet, 30% titanium mineral, and 25% sillimanite and magnesite) (Angusamy et al., 2005). Pichavaram area (11°24'59.8"N 79°47'55.8"E) is located in Cuddalore district, Tamil Nadu, India. The geology of Cuddalore is filled with black clay, silty clay, red clayey sand, conglomerate, and calcareous sandstone and is made up of sedimentary rock formations as shown in figure. 1. The study area is made of quaternary and laterite deposits along the region with the boundary of AVIRIS-NG data as shown in figure. 2. The abundant minerals present in this region are clay, silicate, and iron oxide-based minerals (Angusamy et al., 2005; Ravisankar et al., 2012). The study area in this work explores the following minerals: vermiculite, antigorite, diopside, rectorite, and ammonio jarosite. The SAM and SFF methods confirmed the presence of minerals.

Dataset description

The AVIRIS-NG dataset used in this study was obtained on March 4th, 2018, as part of collaboration between JPL NASA with ISRO campaign. It is a cutting-edge HSI sensor that can produce hyperspectral images of 425 continuous bands in the 380 nm-2510 nm range with a better spectral resolution of 5 nm (NASA, 2015). The collected data has a spatial resolution of 8.1 meters. The details of the AVIRIS-NG dataset utilised in the investigation are presented in Table 1.

Table 1. AVIRIS-NG Data Specifications

Parameters	Range
Sensor Altitude	4-8 km
Spatial Resolution	8.1m
Swath Width	4-6 km
VNIR Range	400 nm- 1000 nm
IFOV (mrad)	1.0 mrad
Spectral Range	380 nm -2500 nm
Spectral Coverage	Continuous
Spectral Resolution	5 nm
SWIR Range	900 nm – 2500 nm
Total number of bands	425

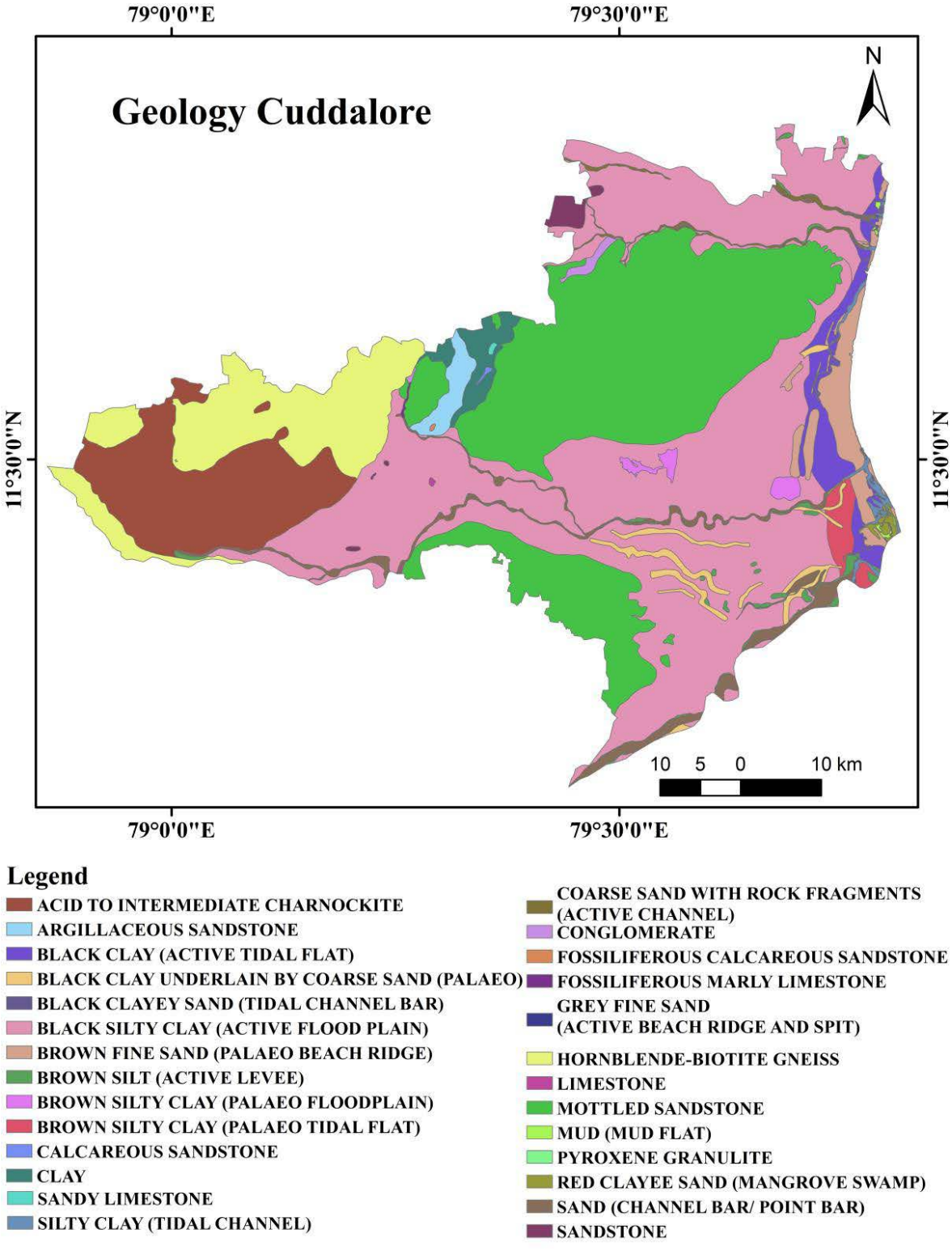

Figure 1. represents the geology map of cuddalore region

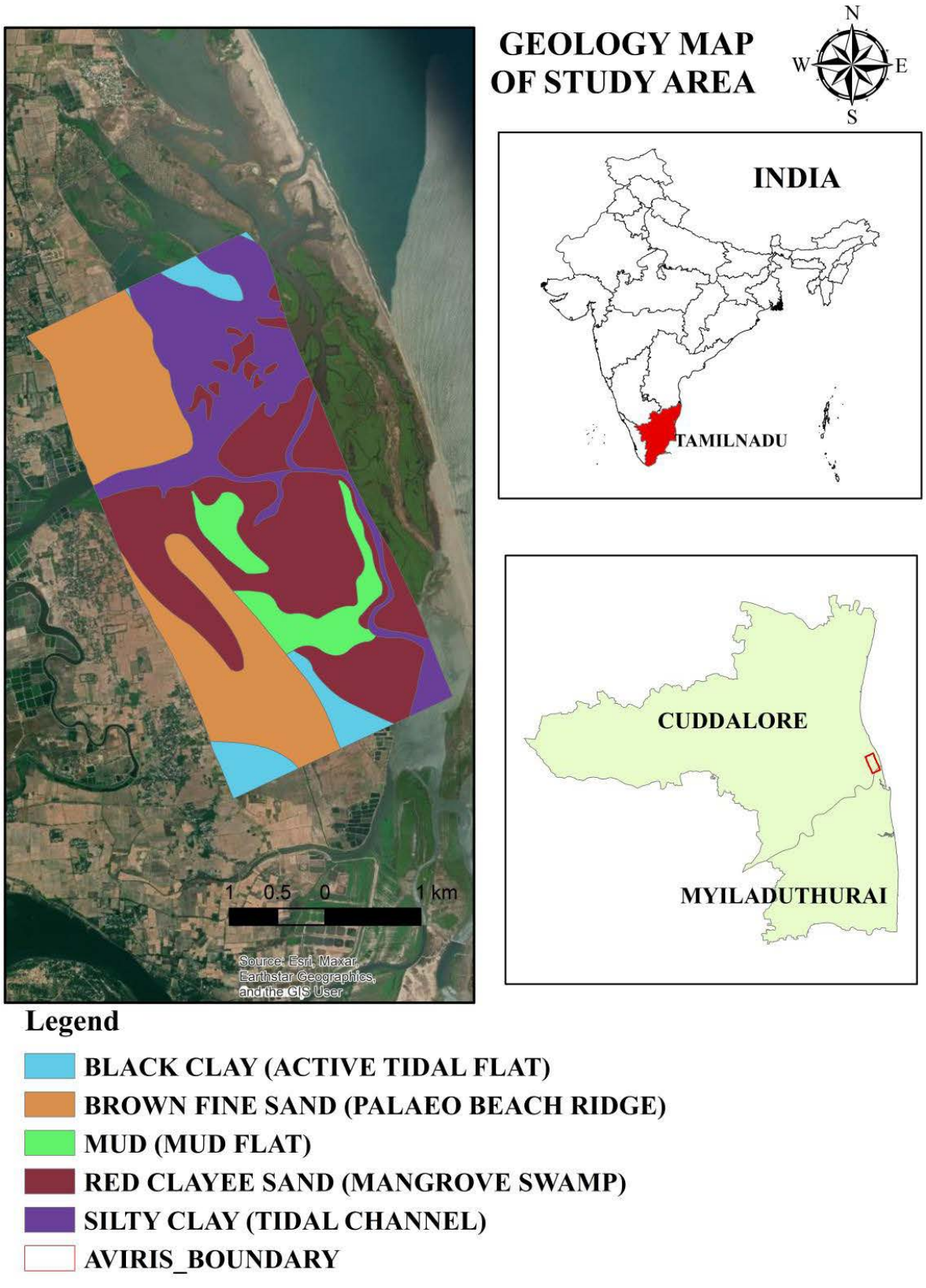

Figure 2. Geology map of the study area with the AVIRIS-NG data

Data and methodology

AVIRIS-NG data have a high SNR when compared with the Hyperion data (Tripathi and Govil, 2019). Some initial steps involved in the preprocessing of images include atmospheric correction, noisy band removal, and radiometric calibrations. AVIRIS-NG extracted image spectra were verified with a calibrated USGS spectral library. The following phase entails identifying minerals based on their wavelength reflectance curves and absorption feature depths at various wavelengths using subjective image interpretation. The reflectance bands extracted from AVIRIS-NG images were compared with the USGS mineral spectral database for mineral analysis. In the process of mineral identification, the steps involved in the processing of AVIRIS-NG data are shown in the figure.3.

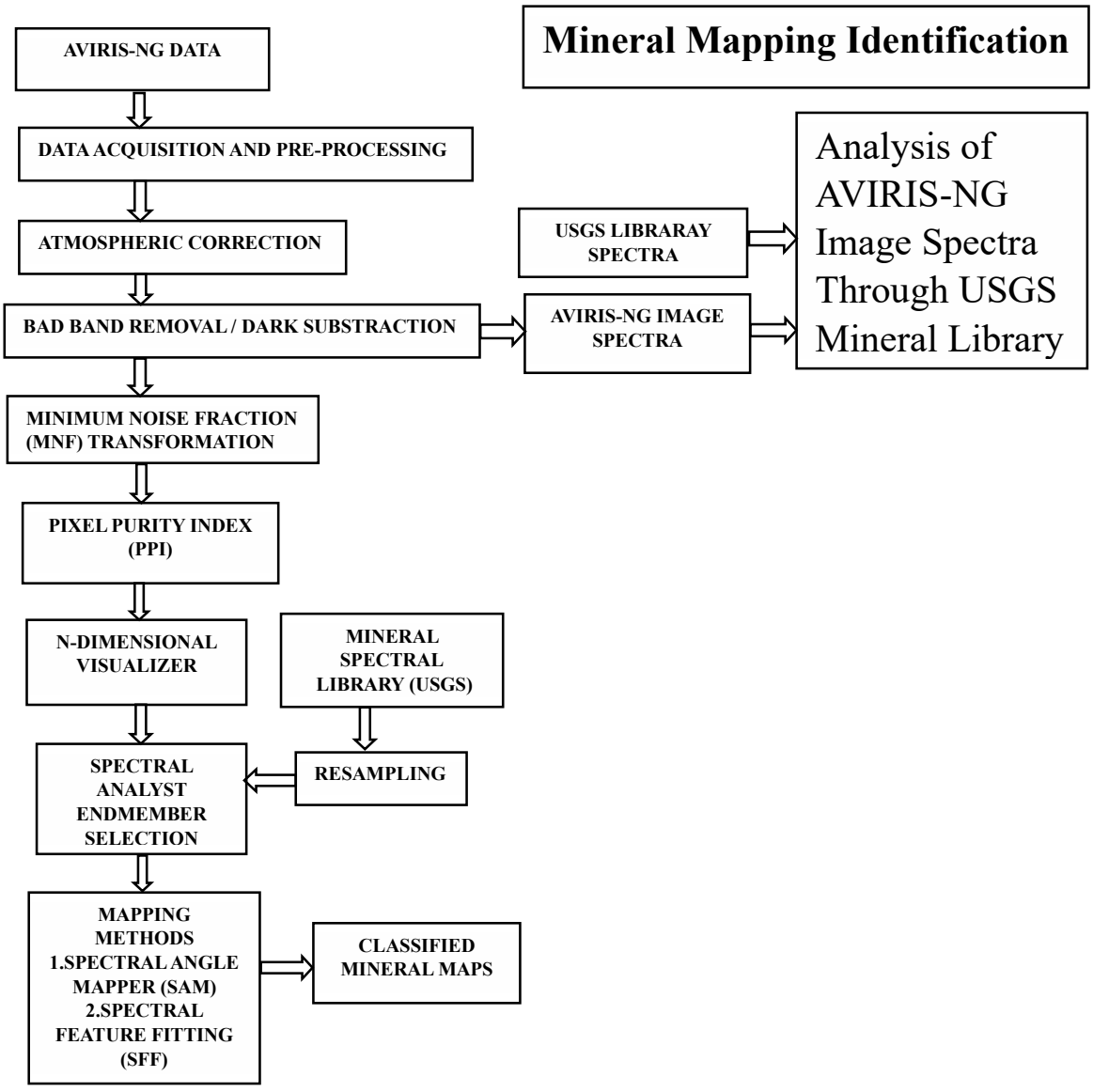

Figure 3. Flow diagram of the mineral mapping identification

Preprocessing of AVIRIS-NG data

Many closely spaced bands in the hyperspectral information leads to radiometric errors. Image rectification requires the preprocessing of hyperspectral data. The data set provided has been exploited in its original, unprocessed state. The data obtained from the agency needs to be corrected for radiometric, geometric, or atmospheric factors. The data collection needs to be corrected due to atmospheric effects. Atmospheric adjustment and radiometric calibration are necessary. The smile effect does not affect the AVIRIS-NG data set due to its better SNR (Hamlin et al., 2011; Thorpe et al., 2016; Govil et al., 2018b).

Atmospheric correction

A remote sensing sensor captures the radiant energy that travels from the sun to the earth's surface, then from the earth to the sensor, passing through the earth's atmosphere. Obtaining the accurate reflectance energy of an item on the earth's surface necessitates specific atmospheric coefficients for atmospheric correction. Compensating for atmospheric coefficients such as surface altitude, surface albedo, aerosol, water vapour column, surface and atmospheric temperatures, cloud optical depths, and scene visibility is necessary to obtain ground reflectance (Adler-Golden et al., 1994). Water vapour estimation is calculated independently for each pixel in AVIRIS-NG images during the atmospheric correction.

FLAASH

The FLAASH model operates based on a conventional equation for spectral radiance at a sensor pixel, specifically for flat Lambertian materials, L (FLAASH User' S Guide, 2005). The equation is given as –

$$L=\left(\frac{A\rho}{1-\rho_e S}\right)+\left(\frac{B\rho_e}{1-\rho_e S}\right)+L_a \quad (1)$$

Where- ρ – "Pixel surface reflectance"; ρ_e- "Radiance at sensor Atmospheric spherical albedo"; L_a- "Backscattered radiance by atmosphere"; "A & B are coefficients" (which depend upon atmospheric and geometric condition).

MNF transformation

The hyperspectral imagery contains a large amount of data, leading to extensive data processing and sophisticated computations (Mondal et al., 2022). MNF reduces the dimensionality of data from a higher to a lower level while retaining all the information with higher eigen values for the initial bands as shown in figure.4. MNF transform is mainly used to extract and separate the majority of endmembers pixel information from the random noise thus by reducing the data dimensionality without losing the accurate signal information

from the image data (Guha, 2020). The MNF transformation method was created by Green et al., in 1988 to reduce dimensionality and qualitatively analyze images by transforming image components into a meaningful sequence.

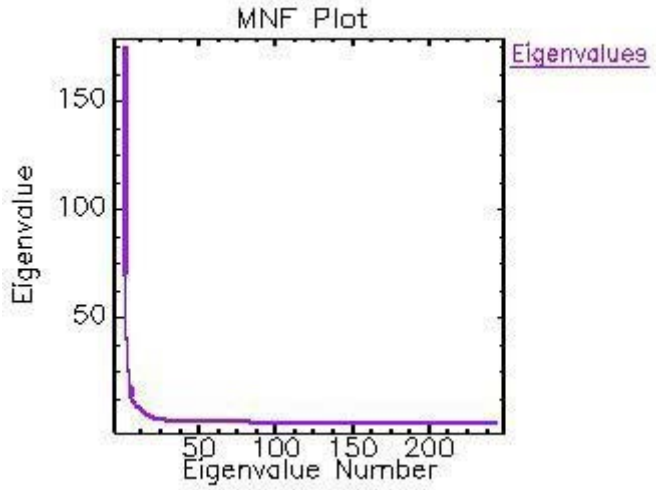

Figure 4. MNF plot showing bands having higher eigenvalues

End member extraction

The spectral endmembers are extracted from the AVIRIS-NG data using the spectral hourglass approach in ENVI, which involves some standard methods of MNF, PPI, and N-D visualizer. According to Van Der Meer et al., (2011), the PPI is the best method to extract the pure pixel from the MNF image. Usually, PPI is computed automatically using the higher eigenvalues from MNF data through convex geometry, which is possible by repeated projections on the N-D scatter plots. The brightness of pixels in the PPI image indicates the higher relative purity with recording of extreme pixels. Evaluating end member determination involves creating a scatter plot of 10,000 projections and applying a 2.5 threshold factor to the MNF band picture to isolate purer materials from mixed ones and pick the purest PPI pixels as shown in figure.5.

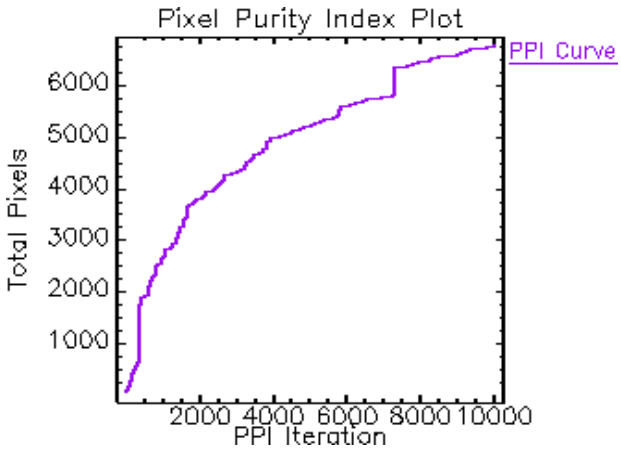

Figure 5. PPI method to extract the pure pixel

In Image classification, extracting pure pixel spectra plays a vital role in identifying and mapping minerals through the spectral mixing concept of the N-D visualizer (Boardman and Kruse, 2011). The extreme pixels with higher values are chosen as regions of interest (ROI) from the N-D visualizer as shown in figure. 6. The pure pixel and spectra are recovered using an N-D visualizer approach applied to the ROI on the MNF image (Boardman et al., 1995). The spectral reflectance curves are derived through atmospheric correction of calibrated images by comparing the spectra with the USGS standard spectral library (Nahry and Altinbas, 2006).

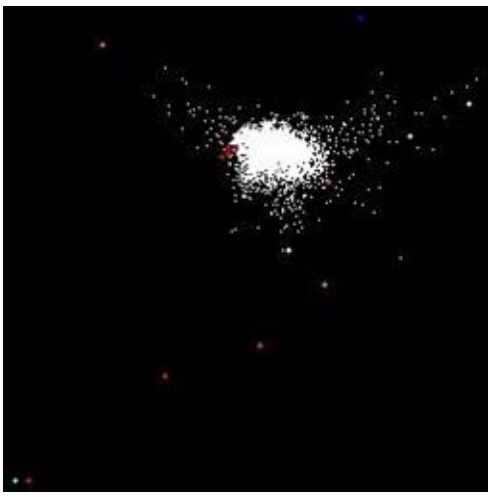

Figure 6. N-D visualizer for identification of endmembers

SAM Algorithm

SAM techniques, which evaluate the similarity between reference and image spectrum by calculating the spectral angle between two vectors with the exact origin as given 247 in equation (2), are used to identify minerals (Guha, 2020).

$$\cos\varphi = \frac{\sum_{i=1}^{n} e_i r_i}{\sqrt{\sum_{i=1}^{n} e_i^2}\sqrt{\sum_{i=1}^{n} r_i^2}} \tag{2}$$

Spectral feature fitting (SFF)

SFF matches the absorption features of reference spectra with the obtained image spectra (Van Der Meer, 2004). The most important point of SFF is based on the correlation coefficients of the original image pixel spectrum (S) and Continuum (C) Curve, as shown in equation (3) and their results in the figure.7.

$$\text{SCR} = S/C \tag{3}$$

Where SCR- “Continuum removed spectra”,

S – “Original spectra”,

C- “Continuum curve”.

SFF provides information for forecasting each pixel's absorption characteristics' structure and magnitude (Guha, 2020).

RESULTS AND DISCUSSION

At the location of the Pichavaram region, the spectral reflectance curve of clay, silicate, and iron-oxide-based minerals shows different deep absorption features at specific wavelengths based on mineral category (Angusamy et al., 2005; Guha, 2020).

Clay minerals usually have an absorption feature in the SWIR region due to the vibration of molecular bonds that mainly occur in combinations like the bending of metal-OH bonds and the stretching of O-H bonds—the absorption features of clay minerals at 1400 nm and 1900 nm (Fan et al., 2012; Guha, 2020). The different clay minerals will have absorption features to locate the precise and identify the minerals in the spectral range of 2100 nm – 2300 nm (Guha, 2020). The six minerals classified in this work are vermiculite, antigorite, rectorite, diopside, and ammonio jarosite.

Vermiculite is a type of clay mineral with a vital absorption feature at 1900 nm and a weak absorption feature at 2200 nm is shown in figure.7. (a) and also, it has excellent positive correlation absorption depth at 900 nm -1000 nm. Due to the multiple water molecules in the minerals, the combination of O-H-O and OH bonds create stronger absorption features from 1000 nm to 2300 nm wavelengths than metal-OH bonds (Guha, 2020).

Antigorite is classified under a non-clay phyllosilicate structure based mineral category and belongs to the serpentine group (Fan et al., 2012). It has a vital absorption feature at 1400 nm and 2300 nm as shown in figure.7. (b). The absorption depth is very similar and comparable to clay minerals (Guha, 2020).

The contribution of silicate-based minerals to the earth's planet is about 90%, and they also play an important role in classifying minerals (Fan et al., 2012). Minerals like rectorite and diopside are used in this analysis. Minerals' absorption features exist in the range of 1000 nm — 2400 nm wavelength (Guha, 2020).

Rectorite minerals are classified under the structure of phyllosilicate of clay mineral group (Fan et al., 2012). Figure. 7. (c) produces the robust absorption features are available at 1400 nm, 1910 nm, and 2200 nm to 2400 nm wavelengths.

Diopside is classified as an inosilicate mineral in the silicate-based mineral category and belongs to the Pyroxene group (Fan et al., 2012). Its absorption features are available in the range of 400 nm—2300 nm. Robust absorption features are available at 1100 nm, and moderate absorption features are available at 2200 nm, as shown in the figure.7. (d).

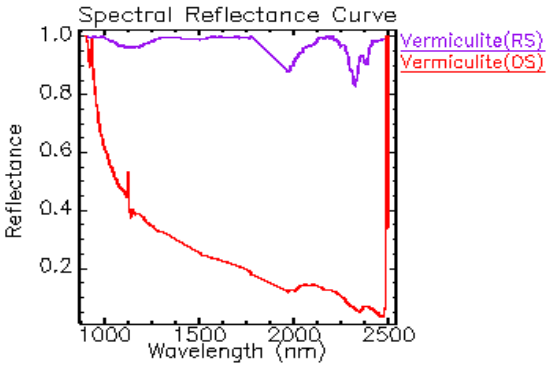

(a)

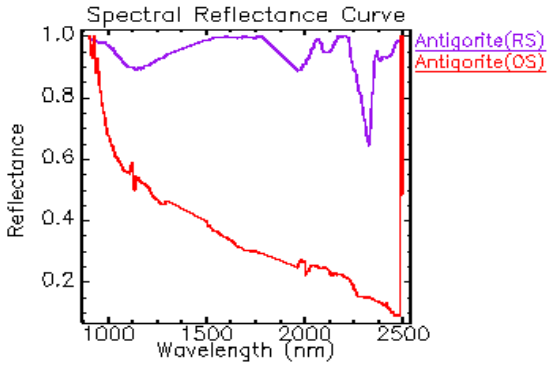

(b)

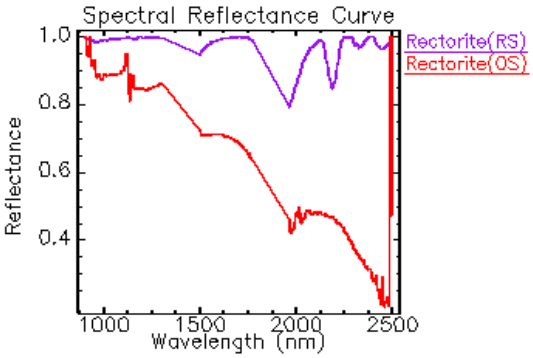

(c)

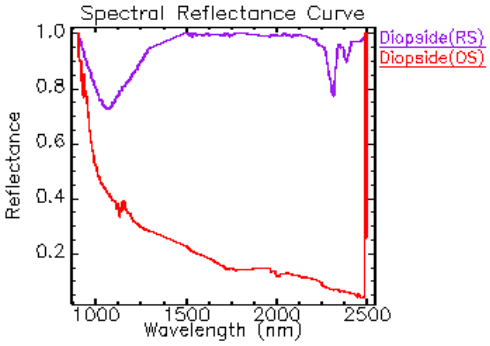

(d)

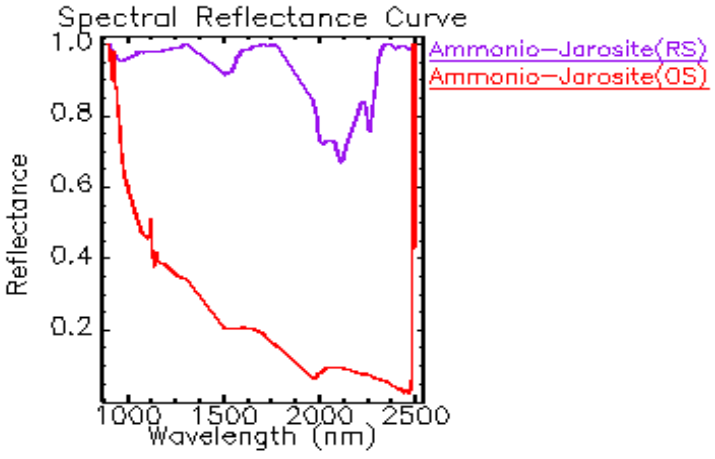

(e)

Figure 7. Reflectance mineral spectrum and obtained mineral spectrum of (a) vermiculite, (b) antigorite, (c) rectorite, (d) diopside, & (e) ammonio jarosite

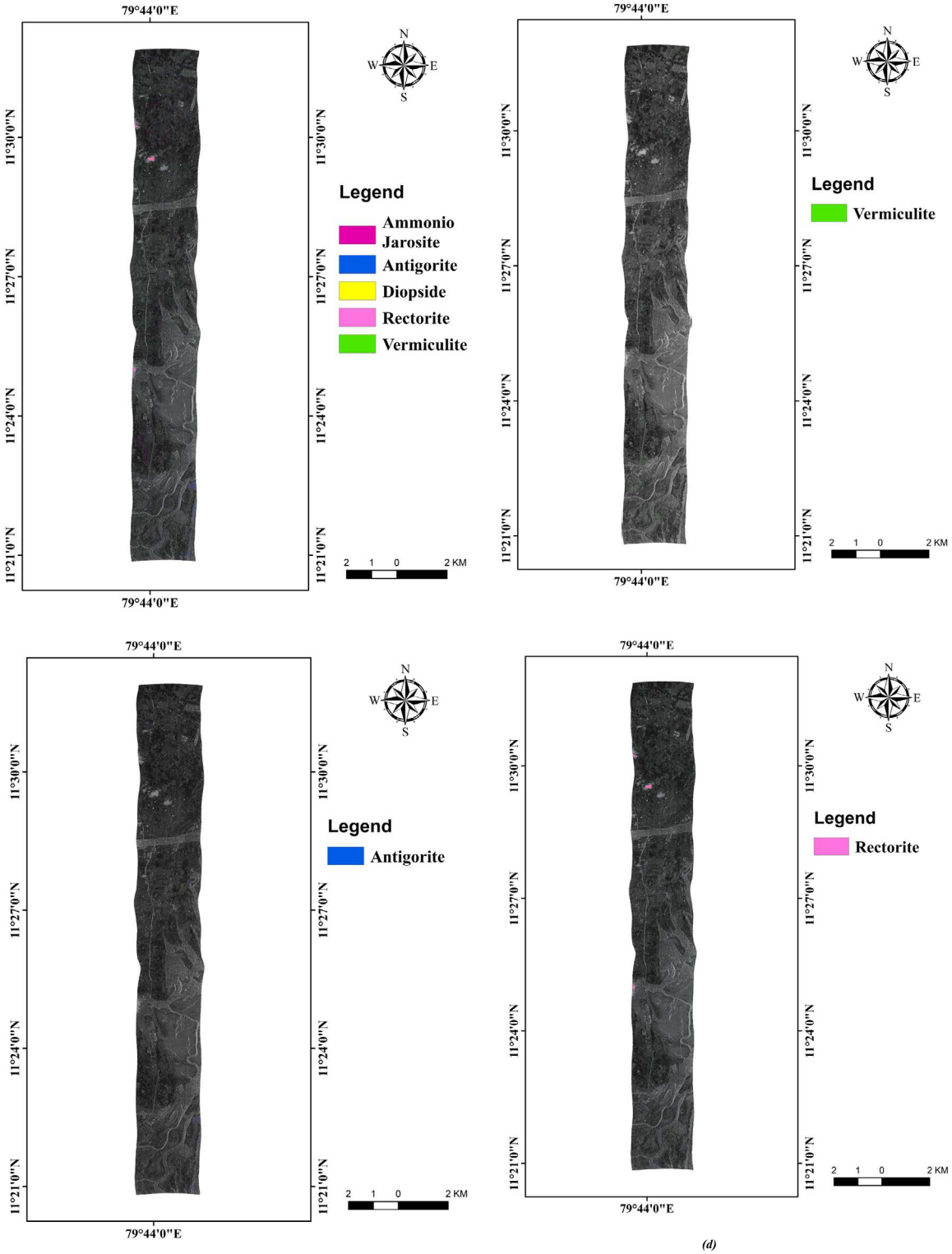
79°44'0"E
11°30'0"N
11°27'0"N
11°24'0"N
11°21'0"N
N
W
E
S
Legend
Ammonio Jarosite
Antigorite
Diopside
Rectorite
Vermiculite
2 1 0 2 KM
(c)
Legend
Vermiculite
(d)
Legend
Antigorite
Legend
Rectorite

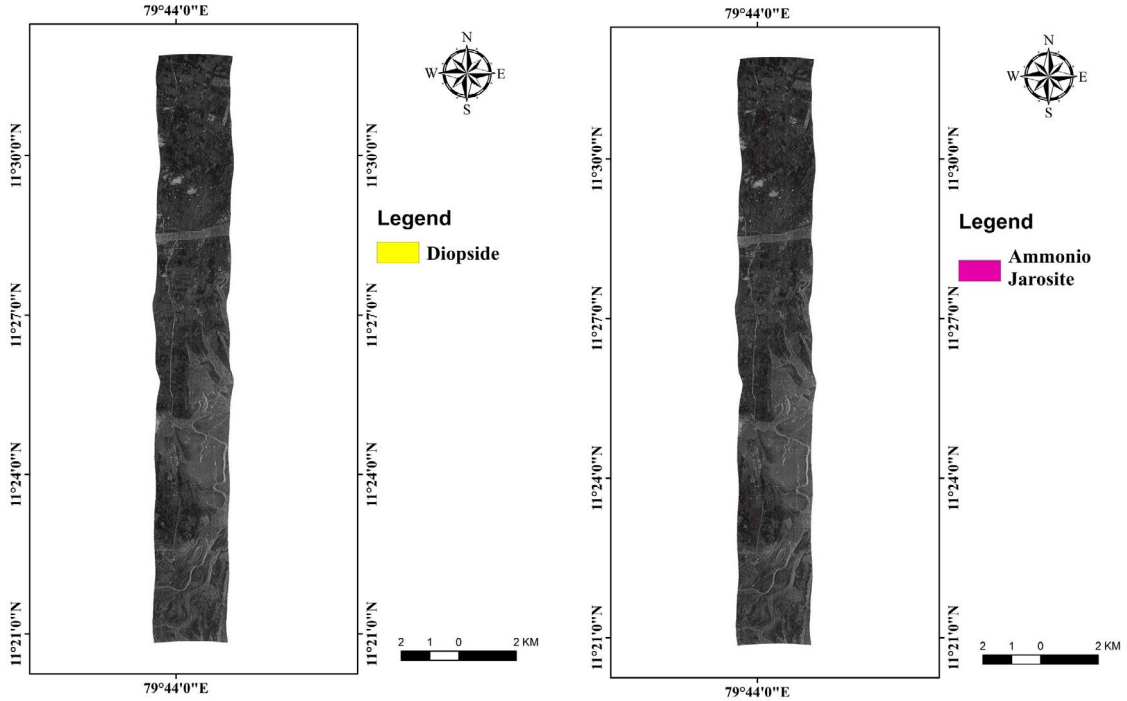

Figure 8. Shows the SAM classified mineral maps for (a) mineral map distribution of pichavaram region (b) vermiculite, (c) antigorite, (d) rectorite, (e) diopside, & (f) ammonio jarosite

Ammonio jarosite is classified under the iron oxides-based mineral category and belongs to the jarosite group (Fan et al., 2012). The absorption features are available at 910 nm, 1470 nm, 1940 nm, and 2270 nm wavelengths, which will be used to locate the jarosite mineral in the hyperspectral sensing data, as shown in the figure.7. (e). The above range of features are used to locate precise mineral classifications in the spectral domain. The minerals in the earth and other planets can be identified using the chemical properties, structure and absorption feature depths (Guha, 2020).

The mineral maps are prepared from the AVIRIS-NG hyperspectral data by analysing 250 out of 425 bands after the radiance conversion to reflectance. The bands have been selected from the range of 400 nm –2500 nm. Most of the information available in the first 16 bands is chosen with higher eigenvalues with a dimensionality of 10, and the rest of the bands contained noise in the dataset. The specific absorption features are identified in the following regions are 400 nm –2500 nm. Eight endmembers are extracted after the processing of the image, which involves the following minerals such as a, vermiculite, antigorite, rectorite, diopside, and ammonio jarosite.

SAM algorithm has been used to compare the similarity of the obtained image spectra from the image with the USGS reference spectral available in the ENVI library. The map for the particular mineral is generated based on the higher threshold value of SAM for classification. The threshold values for, vermiculite, antigorite, rectorite, diopside, and ammonio jarosite are, 0.06, 0.07,

0.06, 0.07, and 0.05 radians. In the SAM classified image, different colours are mapped as shown in Figure 8, green for vermiculite, blue for antigorite, pink for rectorite, yellow for diopside, and magenta for ammonio jarosite.

Finally, the classified map of SAM and spectral reflectance curve of SFF classified the same minerals, which resulted in better accuracy in predicting the mineral location using the AVIRIS-NG hyperspectral data.

CONCLUSIONS

Clay (vermiculite), silicate (antigorite, rectorite, diopside) and iron-oxide (ammonio jarosite) minerals are explored using the AVIRIS-NG hyperspectral data. The obtained reflectance spectrum results matched the USGS spectral library spectra in the ENVI software. Vermiculite shows a result of a vital absorption feature at 1900 nm and a weaker absorption feature at 2200 nm, mainly because of higher SNR and better spectral /spatial resolution available in AVIRIS-NG data. The antigorite mineral shows a more robust diagnostic absorption at 1400 nm and 2300 nm, which are similar and comparable to clay minerals. The rectorite minerals show strong absorption features at 1400 nm,1910 nm, and 2200 nm to 2400 nm wavelengths. The diopside minerals show stronger absorption features at 1100 nm and moderate at 2200 nm. Finally, the iron-oxide-based mineral of ammonia jarosite shows that the absorption features are available at 910 nm, 1470 nm, 1940 nm, and 2270 nm wavelengths. The spectral reflectance curve obtained from the AVIRIS-NG data shows excellent similarity and accuracy with the reference spectral curve from the USGS library.

The SAM algorithm is used to prepare the mineral map. The minerals present in the Pichavaram region are classified into vermiculite, antigorite, rectorite, diopside, and ammonio jarosite. The SFF algorithms show an excellent similarity between the reflectance curve's absorption feature and the depth of the above-listed minerals. This study shows that excellent mapping of minerals using AVIRIS-NG data has higher reliability and detailed analysis of minerals. Airborne sensors of AVIRIS-NG data prove to have good efficiency and achieve high accuracy because of higher SNR and high spectral/spatial resolution compared to other space-borne sensors. The results prove to be one of the best methods to identify mapping of minerals using AVIRIS-NG data.

REFERENCES

Adler-Golden, S., Beryl, A., Bernstein, L.S., Richtsmeierl, S., Acharyal, P.K., Matthew,

M.W., Anderson, G.P., Allred, C.L., Jeong, L.S., Chetwynd, J.H.,1994, FLAASH, A Modtran4 Atmospheric Correction Package.

Agrawal, N., Govil, H., Chatterjee, S., Mishra, G., and Mukherjee, S., 2024, Evaluation of machine learning techniques with AVIRIS-NG dataset in the identification and mapping of minerals. Advances in Space Research,

v.73(2), pp.1517–1534. doi: https://doi.org/10.1016/j.asr.2022.09.018

Angusamy, N., Sahayam, J. D., Gandhi, M. S., and Rajamanickam, G. V., 2005, Coastal placer deposits of central Tamil Nadu, India. Marine Georesources & Geotechnology, v.23(3), pp.137–174. doi: https://doi.org/10.1080/10641190500192102

Boardman, J. W., and Kruse, F. A., 2011, Analysis of imaging spectrometer data using Dimensional geometry and a Mixture-Tuned Matched filtering approach. IEEE Transactions on Geoscience and Remote Sensing, v.49(11), pp.4138–4152. doi: https://doi.org/10.1109/tgrs.2011.2161585

Boardman, J. W., Kruse, F. A., and Green, R. O.,1995, Mapping target signatures via partial unmixing of AVIRIS data. Jet Propulsion, Lab v.23. doi: https://ntrs.nasa.gov/api/citations/19950027316/downloads/19950027316.pdf

Fan, C., Xie, H., Wu, J., and Birnbaum, S. J., 2012, Analysis of United States Geological Survey spectral library of silicate minerals: implication for remote sensing applications. Journal of Applied Remote Sensing, v.6(1), 063514. doi: https://doi.org/10.1117/1.jrs.6.063514

FLAASH User' s Guide.,2005, ENVI Documentation. Girija, R. R., and Sundararajan, M., 2019, Mapping of mineral resources and lithological units: a review of remote sensing techniques. International Journal of Image and Data Fusion, v.10(2), pp.79–106. doi: https://doi.org/10.1080/19479832.2019.1589585

Govil, H., Tripathi, M. K., Diwan, P., Guha, S., and Monika., 2018a, Identification of iron oxides minerals in western Jahajpur region, India using AVIRIS-NG hyperspectral remote sensing. The International Archives of the Photogrammetry, Remote Sensing and Spatial Information Sciences, v. XLII–5, pp.233–237. doi: https://doi.org/10.5194/isprs-archives-xlii-5-233-2018

Govil, H., Tripathi, M. K., Diwan, P., Guha, S., and Monika., 2018b, Identification of iron oxides minerals in western Jahajpur region, India using AVIRIS-NG Hyperspectral remote sensing. The International Archives of the Photogrammetry, Remote Sensing and Spatial

Information Sciences, v.XLII–5, pp.233–237. doi: https://doi.org/10.5194/isprs-archives-xlii-5-233-2018

Govil, H., Tripathi, M. K., Diwan, P., and Monika., 2019, Comparative evaluation of AVIRIS- NG and Hyperion Hyperspectral image for TALC mineral identification. Advances in intelligent systems and computing, pp. 95–101. doi: https://doi.org/10.1007/978-981-13- 9364-8_7

Green, A., Berman, M., Switzer, P., and Craig, M.,1988, A transformation for ordering multispectral data in terms of image quality with implications for noise removal. IEEE Transactions on Geoscience and Remote Sensing, v.26(1), pp.65–74. doi: https://doi.org/10.1109/36.3001

Guha, A., 2020, Mineral exploration using hyperspectral data. In Elsevier eBooks, pp. 293– 318. doi: https://doi.org/10.1016/b978-0-08-102894-0.00012-7

Hamlin, L. A., Green, R. O., Mouroulis, P., Eastwood, M. L., Wilson, D.

W., Dudik, M. J., and Paine, C., 2011, Imaging spectrometer science measurements for Terrestrial Ecology: AVIRIS and new developments. IEEE Aerospace Conference Proceedings. doi: https://doi.org/10.1109/aero.2011.5747395

Kumar, C., Chatterjee, S., Oommen, T., and Guha, A., 2020, Automated lithological mapping by integrating spectral enhancement techniques and machine learning algorithms using AVIRIS-NG hyperspectral data in Gold-bearing granite-greenstone rocks in Hutti, India. International Journal of Applied Earth Observation and Geoinformation, v.86. doi: https://doi.org/10.1016/j.jag.2019.102006

Mishra, G., Govil, H., Guha, A., Kumar, H., Kumar, S., and Mukherjee, S., 2024, Comparative evaluation of airborne AVIRIS-NG and spaceborne PRISMA hyperspectral data in identification and mapping of altered/weathered minerals in Jahazpur, Rajasthan. Advances in Space Research, v.73(2), pp.1459–1474. doi: https://doi.org/10.1016/j.asr.2022.09.047

Mondal, S., Guha, A., and Pal, S. K., 2022, Comparative analysis of AVIRIS-NG and Landsat-8 OLI data for lithological mapping in parts of Sittampundi layered complex, Tamil Nadu, India. Advances in Space Research, v.69(3), pp.1408–1426. doi: https://doi.org/10.1016/j.asr.2021.11.001

Nahry, and Altinbas., 2006, Processing and analyzing advanced hyperspectral imagery data for identifying clay minerals. A case study. Journal of Applied Science Research, v.2(4), pp.232–238.

NASA AVIRIS–NG, 2015, Airborne flights over India Science Plan document for hyperspectral remote sensing. Oskouei, M. M., and Babakan, S., 2016, Detection of alteration minerals using hyperion data analysis in Lahroud. Journal of the Indian Society of Remote Sensing, v.44(5), pp.713–721. https://doi.org/10.1007/s12524-016-0549-6

Peyghambari, S., and Zhang, Y., 2021, Hyperspectral remote sensing in lithological mapping, mineral exploration, and environmental geology: an updated review. Journal of Applied Remote Sensing, v.15(03). doi: https://doi.org/10.1117/1.jrs.15.031501

Priya, S., and Ghosh, R., 2024, Soil clay minerals abundance mapping using AVIRIS-NG data. Advances in Space Research, v.73(2), pp.1360–1367. doi: https://doi.org/10.1016/j.asr.2022.09.049

Ravisankar, R., Eswaran, P., Rajalakshmi, A., Chandrasekaran, A., Thillaivelavan, K. K., and Dhinakaran, B.,2012, Beach Rocks from the South East Coast of Tamilnadu, India: A Spectroscopic Study. Pelagia Research Library, v.3(1), pp.95–102. doi: https://www.pelagiaresearchlibrary.com

SAC, 2016, Space Application Center.pdf (3rd ed., Vol. 41). SAC Cour. Thorpe, A. K., Frankenberg, C., Aubrey, A. D., Roberts, D. A., Nottrott, A., Rahn, T., Sauer, J. A., Dubey, M. K., Costigan, K. R., Arata, C., Steffke, A., Hills, S. J., Haselwimmer, C.,

Charlesworth, D., Funk, C. C., Green, R., Lundeen, S., Boardman, J. W., Eastwood, M. L., McFadden, J. P., 2016, Mapping methane concentrations from a controlled release experiment using the next generation airborne

visible/infrared imaging spectrometer (AVIRIS-NG). Remote Sensing of Environment, v.179, pp.104–115. doi: https://doi.org/10.1016/j.rse.2016.03.032

Tripathi, M. K., and Govil, H., 2019, Evaluation of AVIRIS-NG hyperspectral images for mineral identification and mapping. Heliyon, v.5(11), pp.29-31. doi: https://doi.org/10.1016/j.heliyon.2019.e02931 Van Der Meer, F. D., 2004, Analysis of spectral absorption features in hyperspectral imagery. International Journal of Applied Earth Observation and Geoinformation, v. 5(1), pp. 55–68. doi: https://doi.org/10.1016/j.jag.2003.09.001

Van Der Meer, F., Van Der Werff, H., Van Ruitenbeek, F., Hecker, C., Bakker, W., Noomen, M., Van Der Meijde, M., Carranza, E. J. M., De Smeth, J., and Woldai, T., 2011, Multi - and hyperspectral geologic remote sensing: a review. International Journal of Applied Earth Observation and Geoinformation, v.14(1), pp.112-128. doi: https://doi.org/10.1016/j.jag.2011.08.002